ASME Journal of Electrochemical Energy Conversion and Storage
Online journal at:
https://asmedigitalcollection.asme.org/electrochemical

Vinay Premnath[1]
Electrochemical Safety Research Institutes,
UL Research Institutes,
5000 Gulf Fwy,
UHTB, Bldg 4, Rm 118,
Houston, TX 77204
e-mail: vinay.premnath@ul.org

Mohammad Parhizi
Electrochemical Safety Research Institutes,
UL Research Institutes,
5000 Gulf Fwy,
UHTB, Bldg 4, Rm 118,
Houston, TX 77204
e-mail: mohammad.parhizi@ul.org

Nicholas Niemiec
Electrified Powertrain Section,
Southwest Research Institute,
6220 Culebra Road,
San Antonio, TX 78238
e-mail: nicholas.niemiec@swri.org

Ian Smith
Electrified Powertrain Section,
Southwest Research Institute,
6220 Culebra Road,
San Antonio, TX 78238
e-mail: ian.smith@swri.org

Judith Jeevarajan
Electrochemical Safety Research Institutes,
UL Research Institutes,
5000 Gulf Fwy,
UHTB, Bldg 4, Rm 118,
Houston, TX 77204
e-mail: judy.jeevarajan@ul.org

Characterization of Particulate Emissions From Thermal Runaway of Lithium-Ion Cells

Over the past decade, there has been a significant acceleration in the adoption of lithium-ion (Li-ion) batteries for various applications, ranging from portable electronics to automotive, defense, and aerospace applications. Lithium-ion batteries are the most used energy storage technologies due to their high energy densities and capacities. However, this battery technology is a potential safety hazard under off-nominal conditions, which may result in thermal runaway events. Such events can release toxic gaseous and particulate emissions, posing a severe risk to human health and the environment. Particulate emissions from the failure of two different cell chemistries—lithium iron phosphate (LFP) and nickel manganese cobalt oxide (NMC)—were studied. Experiments were conducted at multiple states of charge (SOC), and three repeats were performed at each SOC for each cell chemistry to examine the repeatability/variability of these events. Particulate emissions were characterized in terms of particulate matter mass (PM2.5), black carbon, and particle number (PN)/size. Failure of a single cell led to a significant release of particulate emissions, with peak emission levels being higher at the higher SOCs. A high level of variability was observed for a specific SOC for LFP cells, while NMCs exhibited relatively less variability. In general, much higher particulate emissions were observed for NMCs compared to LFPs at each SOC. For NMCs at 100% SOC, peak PN levels were ~$2.5 \times 10^{+09}$ particles/cc (part/cc), and black carbon levels were ~60 mg/m^3. For LFPs at 100% SOC, peak PN levels were ~$9.0 \times 10^{+08}$ part/cc, and black carbon levels were 2.5 mg/m^3.
[DOI: 10.1115/1.4065938]

Keywords: lithium-ion batteries, thermal runaway, particulate emissions, energy storage

1 Introduction

Lithium-ion (Li-ion) batteries have significantly impacted our modern world, serving as a vital source of power for a variety of portable electronic devices and electric vehicles, as well as contributing to renewable energy storage systems [1]. Nevertheless, the widespread use of Li-ion batteries has raised concerns about their safety, specifically the risk of thermal runaway events [2]. Thermal runaway can occur due to various off-nominal conditions, including electrical, mechanical, and thermal abuse [3]. Under these conditions, due to the increased internal temperature of Li-ion cells, a series of exothermic chemical reactions are triggered, leading to catastrophic failures, fires, and even explosions of the flammable gases released during this event [4].

Thermal runaway presents a critical safety concern due to the potential venting of gases and the ejection of particulate matter. Characterizing these safety risks is important for various stakeholders, including emergency responders, health researchers, government regulators, and other stakeholders responsible for developing standards and building solutions that advance human safety and sustainability. Research has shown that various gaseous species such as carbon dioxide, carbon monoxide, hydrogen, alkanes, alkenes, acid gases (such as hydrofluoric acid [HF]), and volatile organic compounds (VOCs) are produced during thermal runaway events [5–9]. These gaseous emissions introduce immediate risks, notably the potential for flammability and fire hazards. Accumulation of combustible gases in confined spaces can lead to explosive conditions, increasing the likelihood of fires or explosions. Additionally, VOC emissions can contribute to air pollution, which can have long-term environmental consequences. Some gases such as HF, formaldehyde, nitric oxide, and toluene [9] are highly toxic to human health, evident by their very low immediately dangerous to life and health levels.

[1]Corresponding author.
Manuscript received March 12, 2024; final manuscript received June 6, 2024; published online August 6, 2024. Assoc. Editor: Jun Xu.

While extensive research has been conducted in analyzing gases released during thermal runaway [10], investigation of particulate emissions during thermal runaway events is relatively less explored. Particulate matter emitted during thermal runaway can include materials like metals, metal oxides, carbonaceous soot, and organic chemicals. These emissions can transport toxic and hazardous materials, posing additional health and environmental risks [11]. Depending on their composition, morphology, concentration, and size distribution, these particles can have adverse health effects upon inhalation, contaminate soil and water sources, and impact ecosystems [12]. Moreover, these particles can include high-speed, high-temperature particles that can potentially ignite the flammable gases that are also released, further exacerbating the thermal runaway process [13]. Such particles could also influence and lead to other failure phenomena, such as high-voltage arc discharges, which could have serious consequences. Therefore, understanding and characterizing this ejecta are crucial for both comprehending the dynamics of thermal runaway and mitigating associated health, environmental, and fire risks. Multiple studies have observed the inherent variability of thermal runaway events [14,15]. It is to be noted that the variability in thermal runaway events can directly impact particulate emissions and release profiles during such occurrences.

A few recent studies have focused on characterizing particulate emissions during thermal runaway. The focus of all these studies has been on larger particulates (>2.5 μm in size). Zhang et al. [16] conducted an experiment to analyze gaseous and solid particle emissions during thermal runaway of a commercial 50 Ah, 3.65 V nickel manganese cobalt (NMC) cell. Gas chromatography and mass spectrometry (GC–MS) were used to determine the composition of the gases, while particle size analysis, ion chromatography, and inductively coupled plasma mass spectrometry were used for particle emission analysis. They detected 30 elements, most with a size less than 0.5 mm in diameter and a median size of approximately 397 μm. Chen et al. [17] utilized Fourier transform infrared, X-ray diffraction analysis, and GC–MS techniques to characterize the composition of ejected powder during the thermal runaway of an 18650 Li-ion cell. Their findings revealed that the ejected powder mainly consisted of carbon, metals, metal oxides, and organic chemicals. Additionally, the study reported particle size distributions ranging from 8.49 to 300.00 μm in ambient air and 5.94 to 210.04 μm in an Argon atmosphere. Barone et al. [18] utilized scanning electron microscopy (SEM) and energy-dispersive X-ray spectroscopy to investigate the morphology and elemental composition of particulates emitted during thermal runaway incidents in lithium iron phosphate (LFP), NMC, and lithium cobalt oxide batteries. Yang et al. [19] utilized SEM, X-ray fluorescence, and laser particle size analysis to examine the morphology, determine chemical composition, and analyze the particle size distribution of particles emitted during thermal runaway events in NMC cathodes. Furthermore, they investigated the biotoxicity of these particles and compared it to the pristine cathode material. Their study revealed an immediate inhibition of bacterial respiratory activities and observed cell membrane damage following a 5-h exposure to emitted particles. Wang et al. [13] conducted a study investigating particle emissions during the thermal runaway of Li-ion cells with various NMC cathodes. This study examined elemental composition, particle size distribution, morphology, and crystal structure. Their study concluded that most of the particles emitted were less than 0.85 mm and contained elements with potential health and environmental risks. In general, very few studies reported in the literature investigated emissions of smaller particles from battery fires. These particles tend to remain airborne for much longer durations, thereby posing a risk to human health and the environment. Premnath et al. [20] examined fine (less than 2.5 μm) particulate emissions during thermal runaway events in LFP and NMC modules. Their study encompassed measurements of particulate matter mass (PM2.5), real-time particle number and size, as well as real-time black carbon. Notably, their findings revealed emission rates that were 5–6 orders of magnitude higher than those observed in the exhaust of a contemporary heavy-duty diesel engine. This study also demonstrated that a significant release of particles falls well within the respirable size range.

This research program was formulated to address the critical knowledge gap that exists in the literature in understanding fine particulate emissions from battery fires. This program involved examining these emissions from cell-level failure events at different states of charge (SOC) varying from 100% to 10%. Experiments were conducted in triplicates to understand the variability/repeatability of these emissions. Thermal abuse was applied to the test articles in a controlled manner to initiate thermal runaway. Particulate emissions were characterized in detail using multiple state-of-the-art measurement techniques to gain information on black carbon, particle number, and particulate matter emissions. Cells from two different cathode chemistries were studied for pure scientific data gathering and not for comparison between the two chemistries. The results obtained are specific to the cell design, size, and chemistry studied.

2 Experimental Methods

2.1 Test Articles and Test Matrix. This paper focuses on two cell types composed of LFP and NMC cathode chemistries. The NMCs were pouch type, and the LFPs were prismatic metal can type. Both cells considered in this study were fresh cells. The NMC cells were harvested from a module used in an automotive electric vehicle, while the LFP cells were extracted from a battery module used for applications such as energy storage in recreational vehicles, vans, boats, and golf carts. Additional details about the two cell types are listed in Table 1.

The test matrix is shown in Table 2. Three repeats were conducted for each cell type at each SOC. External heating was used as the abuse mechanism, where the test article was heated at a rate of 10 °C/min until the maximum rated temperature of the heater pads was reached (220 °C). Once the peak temperature was achieved, the temperature was held at 220 °C until thermal runaway occurred. The objectives of the test matrix were to examine the repeatability/variability of particulate emissions during thermal runaway and to understand the impact of cell SOC on these emissions. No suppression systems were engaged at any point during these tests, and the thermal runaway event was allowed to unfold naturally.

The LFP cell was instrumented with five thermocouples and four heater pads at various locations, as shown in Fig. 1. One additional

Table 1 Specification of the test articles

Cell type	Specification
LFP cells	Nominal capacity: 50 Ah Nominal voltage: 3.2 V Weight: 1129 g
NMC cell	Nominal capacity: 71 Ah Nominal voltage: 3.7 V Weight: 985 g

Table 2 Test matrix

Cell chemistry	Repeats	State of charge (%)
LFP	1 pilot test	100
LFP	3	100
LFP	3	50
LFP	3	30
LFP	3	10
NMC	1 pilot test	100
NMC	3	100
NMC	3	50
NMC	3	30
NMC	3	10

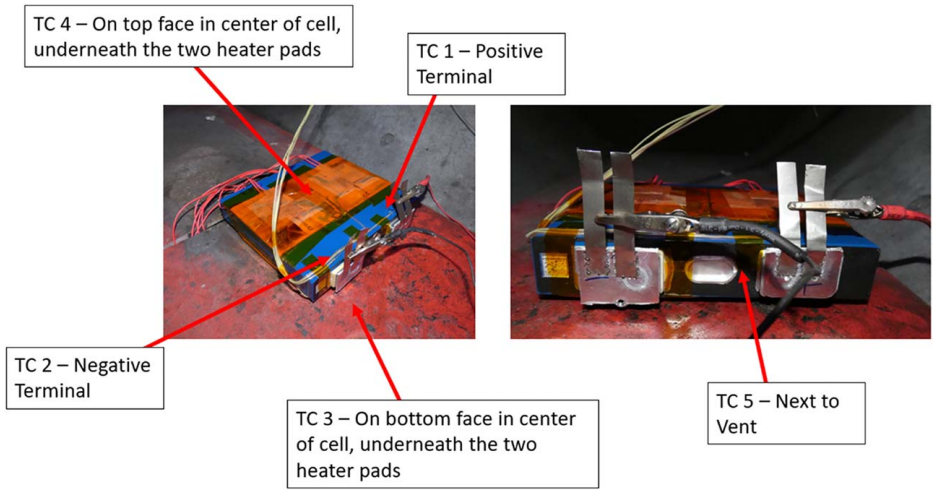

Fig. 1 LFP cell instrumentation and setup

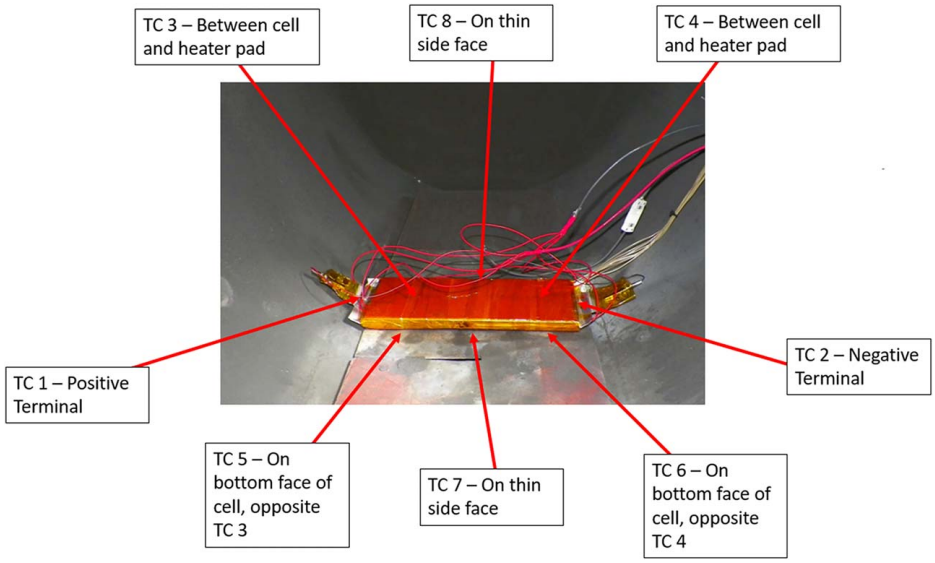

Fig. 2 NMC cell instrumentation and setup

Table 3 Cell conditioning protocol

Cell type	Charging protocol
LFP	Charge at 25 A until 3.6 V, then charge at 3.6 V until the current is less than 1 A Rest for 1 h Discharge at 25 A until 2.5 V Rest for 1 h Charge at 25 A until the desired SOC level based off discharge capacity calculated previously
NMC	Charge at 21.32 A until 4.2 V and then charge at 4.2 V until the current is less than 0.71 A Rest for 1 h Discharge at 35.5 A until 2.7 V Rest for 1 h Charge at 21.32 A until desired SOC level based off discharge capacity calculated previously

thermocouple was used to measure ambient temperature. The cell voltage was also monitored. Details for the NMC cell are shown in Fig. 2. The cell voltage was also monitored. Prior to each test, cells were charged to the test condition using the protocol shown in Table 3.

2.2 Test Chamber, Experimental Setup, and Emissions Analyzers. Testing was conducted in one of the test chambers at SwRI's Energy Storage Technology facility. The test chamber is equipped with a pollution abatement system that enables sampling of particulate and gaseous emissions from Li-ion battery fires. The

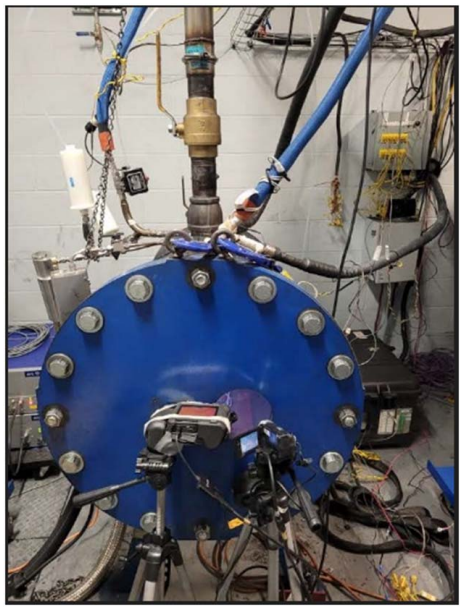

Fig. 3 Test chamber setup

test chamber and the exhaust piping from which particulate measurements were conducted are shown in Fig. 3. The chamber was sealed as much as possible to ensure that any effluents from the thermal runaway process passed through the exhaust piping at the top. Sample probes were installed in the pipe, and stainless-steel transfer lines were used to transport samples to the particulate analyzers. Good aerosol sampling practices were adopted to ensure minimal losses of particulates across the entire sample train from the probe to the instrument. Engineers and technicians controlled and observed the test outside the test cell to ensure personnel safety.

Figure 4 provides a schematic of the test setup. The particle instruments extracted samples from the pipe with a constant air/gas flowrate of ~34.8 lpm. Battery emissions were drawn into the exhaust pipe diluted by air from the ambient environment in the test cell. It is to be noted that sufficient oxygen was always available to sustain combustion.

Detailed characterization of particulate emissions was conducted using the methods described below. It is to be noted that the aerosol sampling techniques used during this program were primarily to measure particles sub-2.5 μm in size—referred to as fine particulates. Battery fires result in the release of larger particulates as well. However, measurement of these emissions was beyond the scope of this program. Characterization of larger particulates requires careful design of isokinetic sample probes and low-loss sampling systems.

2.2.1 Cambustion DMS500 Fast Particle Analyzer. The DMS500 is a real-time nanoparticle size spectrometer that simultaneously measures particle size distribution and number concentration [21]. The instrument can detect and measure particles from 5 nm to 1000 nm in size. The instrument operates on an electrical mobility (size to charge ratio) based classification scheme wherein it charges sample particles using a unipolar corona charger and, subsequently, classifies these particles using twenty-two electrometers based on their electrical mobility (a function of particle charge to size ratio). Signals from these electrometers are processed to generate spectral data on a real-time basis (1 Hz). The instrument also has a built-in dilution system that can be engaged to ensure that the electrometer channels do not get overwhelmed or saturated. For most of the campaign, a dilution setting of ~1500:1 was used.

2.2.2 AVL Micro-Soot Sensor. An AVL micro-soot sensor (MSS), which operates based on a photo-acoustic measurement scheme, was used to measure real-time black carbon concentration [22]. Sample particles are exposed to modulated laser light, which results in an increase in temperature of strongly absorbing black carbon particles. This, in turn, results in the heating of gas surrounding these particles, leading to the generation of sound waves that are detected by a sensitive microphone. This signal is proportional to the concentration of black carbon mass in the measurement chamber. The upper and lower limits of the MSS's detection capability are 50 mg/m^3 and 5 μg/m^3, respectively. The MSS includes an internal dilution system operated at a constant dilution ratio of 3:1.

2.2.3 Gravimetric Particulate Matter Mass Filter Measurement. A Sierra BG-3 partial flow sampling system was used to collect samples on TX40 media 47-mm diameter filters [23]. These filters were pre- and postweighed after sample collection to determine PM emission rate. The BG-3 includes a radial inflow porous stainless-steel dilution tunnel that helps dilute the sample with clean, particulate-free air with minimal losses. The ability to control sample dilution ensures that the filter loading

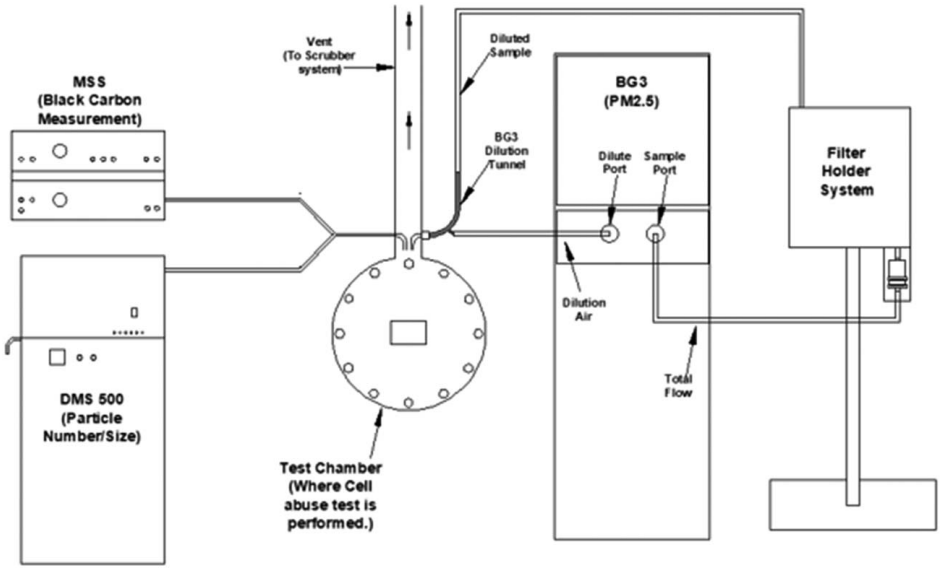

Fig. 4 Schematic of test chamber setup with particulate analyzers

Table 4 Summary of observations for the cell-level abuse test

Battery chemistry	SOC (%)	Round	Peak temperature (°C)	Fire?	Venting location	Pretest weight (g)	Posttest weight (g)
LFP	100	1	373	No	Vent between terminals	1131	920
LFP	100	2	293	No	Vent between terminals	1130	999
LFP	100	3	426	No	Vent between terminals	1127	919
LFP	50	1	271	No	Vent between terminals	1125	944
LFP	50	2	660	Yes	negative terminal	1126	941
LFP	50	3	303	No	back side, negative terminal side[a]	1130	946
LFP	30	1	244	No	back side, negative terminal side[a]	1130	957
LFP	30	2	242	No	Vent between terminals	1135	973
LFP	30	3	227	No	Vent between terminals	1133	997
LFP	10	1	230	No	Vent between terminals	1130	1014
LFP	10	2	231	No	Vent between terminals	1126	994
LFP	10	3	225	No	Vent between terminals	1127	1017
NMC	100	1	1300	Yes	Tabs	982	474
NMC	100	2	1300	Yes	Tabs	983	523
NMC	100	3	1300	Yes	Tabs	981	547
NMC	50	1	697	No	Tabs	980	783
NMC	50	2	754	No	Tabs	983	778
NMC	50	3	768	No	Tabs	981	788
NMC	30	1	576	No	Tabs	984	804
NMC	30	2	570	No	Tabs	982	805
NMC	30	3	561	No	Tabs	983	805
NMC	10	1	342	No	Tabs	982	833
NMC	10	2	384	No	Tabs	982	829
NMC	10	3	307	No	Tabs	981	839

[a]Initial venting accompanied by sparks.

remains within acceptable levels, which would otherwise lead to the filter overloading and tearing (thereby voiding the measurement).

3 Results and Discussion

Results that include physical observations, black carbon emissions, particle number emissions and size signatures, and PM2.5 emissions will be discussed for all cell-level tests conducted as a part of this project. Table 4 summarizes observations made relative to the test article, and Table 5 summarizes particulate emissions data for all tests.

3.1 Physical Observations. All tests were executed using a similar process. Figure 5 serves as an example and provides information on how a specific test was executed from start to finish. Turning on the power to the heater was referred to as the start of the test. It took ~20 min from the start of the test until a peak temperature of 220 °C was reached (also the upper threshold temperature of the heater pads used). Instruments for detecting particulates were placed on stand-by mode once this temperature was reached. This mode prepared the instruments for sampling and led to ambient air being drawn over the test article, thereby resulting in a minor decrease in temperature, as highlighted in the figure. The instruments were placed on "sample mode" once thermal runaway occurred, confirmed visually by venting and by a rapid increase in test article temperatures. The power to the heater pads was turned off during the onset of thermal runaway. Particulate measurements were collected either until the instruments were saturated or until concentrations returned to ambient levels. Following which, a blower system was engaged to evacuate the test chamber and exhaust emissions outside the building after flowing through a filtration/scrubbing system. Engagement of the scrubbing system resulted in a large draw of ambient laboratory air over the test article, thereby cooling it further. The test article was monitored in the test chamber to cool down to temperatures below 50 °C for at least an hour prior to conducting postmortem analysis.

Tables 4 and 5 summarize the results of all the tests conducted in this program. For the LFP chemistry, peak temperatures were highest for 100% SOC, and then steadily decreased as SOC decreased. At 100% SOC, the average peak temperature was 364 °C, and it decreased to an average of 229 °C at 10% SOC. During one of the 50% SOC tests for the LFP chemistry, a fire was observed during thermal runaway, causing a spike in temperature resulting in a peak temperature of ~660 °C (round 2, 50% SOC, LFP test). For most of the LFP testing, venting occurred through the designated vent in the cell. However, for a few tests with 50% and 30% SOC, venting also occurred through the negative terminal, or the back side of the cell, opposite the terminals. Although peak temperatures observed for the NMC cells were much higher, fire was only observed during the 100% SOC tests. At 100% SOC, the thermocouples were destroyed in the fire for the NMC cells, therefore showing temperatures peaking out at the thermocouple limit. As the SOC decreased to 50%, 30%, and 10%, the average peak temperatures decreased to 740 °C, 569 °C, and 344 °C, respectively. For all NMC tests, venting occurred through the seals near the tabs on the cells.

3.2 Black Carbon Emissions. Thermal runaway of both cell chemistries resulted in black carbon emissions. There could be multiple sources for black carbon generation from a Li-ion cell. Graphite, which is a stable form of carbon, is commonly used as the anode active material in Li-ion cells. Carbon additives may also be used in electrodes to enhance electrical conductivity. For events accompanied by combustion and fire, these measurements may also include the emission from combustion. Detailed material characterization of the test articles was beyond the scope of this article and will be included as a part of a future publication. Figure 6 provides real-time black carbon emissions profiles for LFP and NMC tests at various SOCs. Data from one of the repeats at each SOC have been presented in this figure to serve as an example of the release profile after the onset of thermal runaway. Typically, NMC tests resulted in higher black carbon levels than LFP tests. For most tests, peak emission levels were observed close to the onset of thermal runaway. Subsequently, additional excursions in black carbon levels were observed depending on how the event unfolded. For instance, the 100% NMC test yielded a peak close to 40 mg/m^3 early on, and a secondary release after about 75 s with a peak of ~4 mg/m^3. In the case of the 30% LFP test, black carbon activity was observed for ~300 s from the onset of thermal runaway. Environmental

Table 5 Summary of particulate emissions

Battery chemistry	SOC (%)	Round	PM2.5 emissions (g/h)	Black carbon emissions (mg/h)	Particle number emissions (part/h)
LFP	100	Pilot	1.75	0.47	$1.43 \times 10^{+14}$
LFP	100	1	1.78	0.18	$1.63 \times 10^{+14}$
LFP	100	2	1.24	0.02	$1.80 \times 10^{+13}$
LFP	100	3	2.58	0.52	$2.22 \times 10^{+14}$
LFP	50	1	0.28	0.00	$9.71 \times 10^{+12}$
LFP	50	2	1.38	0.17	$9.41 \times 10^{+13}$
LFP	50	3	0.52	0.04	$4.96 \times 10^{+13}$
LFP	30	1	0.94	0.18	$8.96 \times 10^{+13}$
LFP	30	2	0.03	0.00	$5.74 \times 10^{+11}$
LFP	30	3	0.06	0.00	$1.07 \times 10^{+10}$
LFP	10	1	0.05	0.00	$2.03 \times 10^{+10}$
LFP	10	2	0.18	0.00	$4.52 \times 10^{+12}$
LFP	10	3	0.01	0.00	$4.83 \times 10^{+11}$
NMC	100	Pilot	6.73	4.70	$2.89 \times 10^{+14}$
NMC	100	1	3.23	4.15	$1.15 \times 10^{+14}$
NMC	100	2	3.91	4.36	$1.21 \times 10^{+14}$
NMC	100	3	6.49	7.61	$1.25 \times 10^{+14}$
NMC	50	1	2.84	1.35	$1.93 \times 10^{+14}$
NMC	50	2	3.70	1.20	$1.61 \times 10^{+14}$
NMC	50	3	4.05	4.08	$1.73 \times 10^{+14}$
NMC	30	1	3.66	0.28	$5.32 \times 10^{+13}$
NMC	30	2	1.12	0.03	$9.11 \times 10^{+12}$
NMC	30	3	1.26	2.44	$9.31 \times 10^{+13}$
NMC	10	1	0.13	0.00	$4.52 \times 10^{+12}$
NMC	10	2	0.01	0.00	$0.00 \times 10^{+00}$[a]
NMC	10	3	0.01	0.00	$0.00 \times 10^{+00}$[a]

[a]Measured PN concentrations were similar to ambient background levels.

Protection Agency (EPA) guidelines suggest that PM concentrations at or below 12 $\mu g/m^3$ to be safe over a 24-hr exposure window. Levels above 500 $\mu g/m^3$ or 0.5 mg/m^3 are considered to be hazardous to human health. Black carbon is a key component of PM, and peaks of the order of 60 mg/m^3 were observed during some tests.

Figure 7 summarizes observations made for both cell chemistries in terms of average black carbon emissions and peak black carbon emissions observed for all tests conducted. Average emissions have been reported for the first 200 seconds following the onset of a thermal runaway, as the significant release of emissions occurred during this window. LFP tests conducted at a specific SOC exhibited considerable variability, making it difficult to extract a black carbon release trend as a function of SOC. It is to be noted that the variability was intrinsic to the test article, and the abuse test protocol applied for each test was the same. In the case of NMC tests, nominally, higher SOC resulted in higher peak emissions and higher average black carbon emissions. 10% SOC tests did not yield any black carbon emissions for both cell chemistries as the cells did not experience violent venting or thermal runaway. Some of the 30% SOC tests yielded black carbon emissions for both chemistries. In fact, one of the repeats at 30% SOC for the NMC chemistry resulted in a peak close to 7 mg/m^3, which is a significant amount of black carbon emissions.

3.3 Particulate Number Emissions. Particulate number emissions were measured using the DMS500 Fast Particle Sizer. This analytical technique detects all particulate phase emissions ranging from 5 nm to 1000 nm, and simultaneously provides number concentration and size distribution. Figure 8 provides real-time emissions for LFP and NMC tests conducted at different SOCs. High levels of particulate number emissions were observed for both chemistries. Peak levels observed with NMC tests were higher than those of LFP tests conducted at the corresponding SOC. Ambient PN levels in a laboratory setting or inside a house in the US are usually between 2000 and 4000 particles/cc (part/cc). Peak levels observed during the NMC tests were of the order of $2 \times 10^{+9}$ part/cc, which is 6 orders of magnitude higher than ambient levels. LFP tests yielded peak concentrations close to $8 \times 10^{+8}$ part/cc, which is also close to 6 orders of magnitude higher than ambient levels. Typically, the initial release during the onset of thermal runaway resulted in peak PN release levels. During some tests, high PN levels were observed even after the

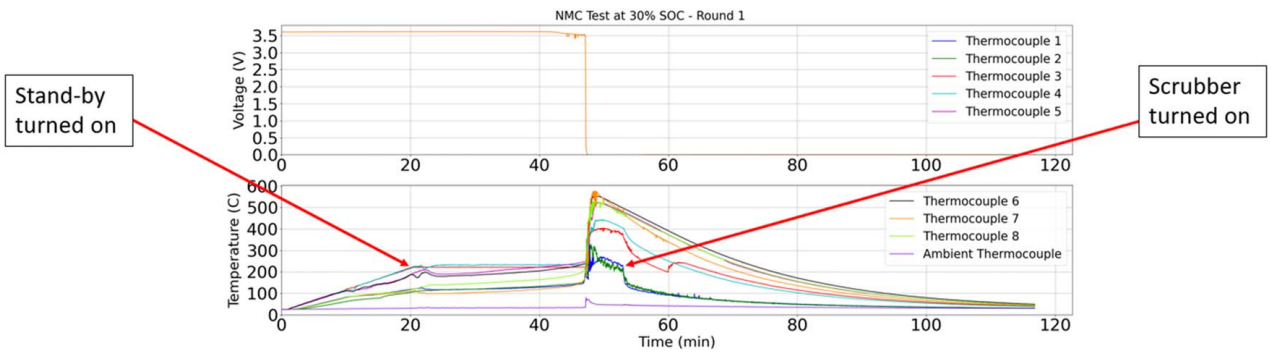

Fig. 5 Example plot outlining test sequence

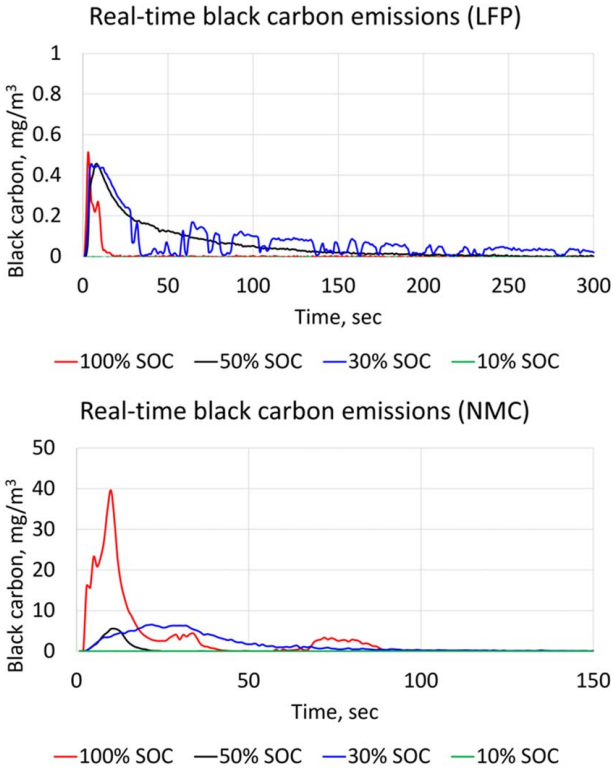

Fig. 6 Real-time profile of black carbon emissions

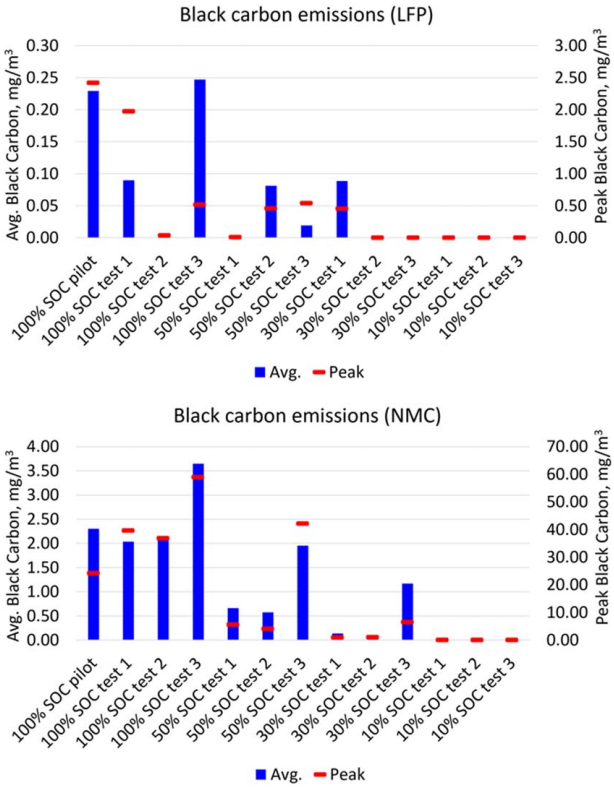

Fig. 7 Average and peak black carbon emissions for all tests

initial release event. It is to be noted that these high PN emissions were from the thermal runaway of a single cell. In real-world applications involving modules and packs composed of multiple cells, these emissions could scale dramatically if propagation of thermal runaway and failure occurs.

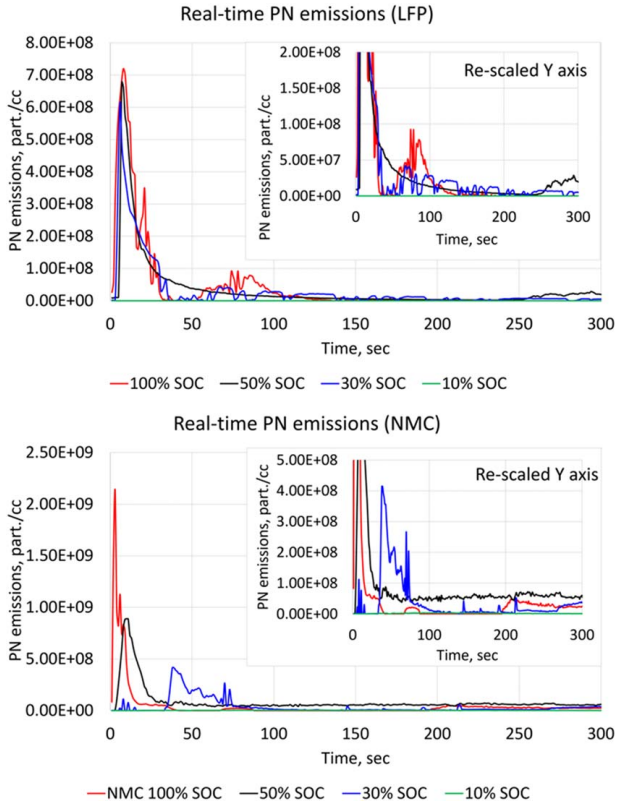

Fig. 8 Real-time profile of particle number emissions

Figure 9 summarizes information for all tests conducted for each cell chemistry at various SOCs. Similar to black carbon analysis, the average concentration observed over the first 200 s from the onset of thermal runaway has been presented. As observed with black carbon emissions, LFP tests exhibited variability in PN emissions as well at specific SOCs. Interestingly, peak PN levels observed during some of the 100%, 50%, and 30% SOC tests were in a similar range of $\sim 8 \times 10^{+8}$ part/cc. No significant PN emissions were observed during the 10% SOC tests. NMC tests resulted in higher PN emissions than LFP tests. In general, peak PN levels decreased with the decrease in SOC, although there were a couple of outliers. While no significant black carbon emissions were observed at 30% SOC for NMCs, significant PN emissions were observed at this SOC. Further, average PN emissions observed during the first 200 s following the onset of thermal runaway were higher for the 50% SOC tests compared to the 100% SOC tests. This was largely due to the release profiles, as shown in Fig. 9. The 100% NMC tests resulted in a very high PN level during the initial release immediately after the onset of thermal runaway, after which PN returned to lower levels. In the case of 50% NMC tests, PN levels remained high even after the initial peak event, as shown in Fig. 8.

3.4 Particulate Matter Mass Emissions. Thermal runaway results in the release of particulate matter composed of various species, including carbonaceous soot, metals, carbonates, and various hydrocarbons, among others. The experimental technique used to characterize PM2.5 emissions from cell abuse involved sampling all ejected constituents on borosilicate glass fiber filters. These filters have very high collection efficiencies and serve as a sensitive technique to better understand thermal runaway emissions. Unlike the other two measurements described in the previous sections, this technique does not generate real-time information. Instead, this batch sampling method was used to determine PM2.5 emissions throughout the entire event. For this program, sample collection on the filter media was performed using a

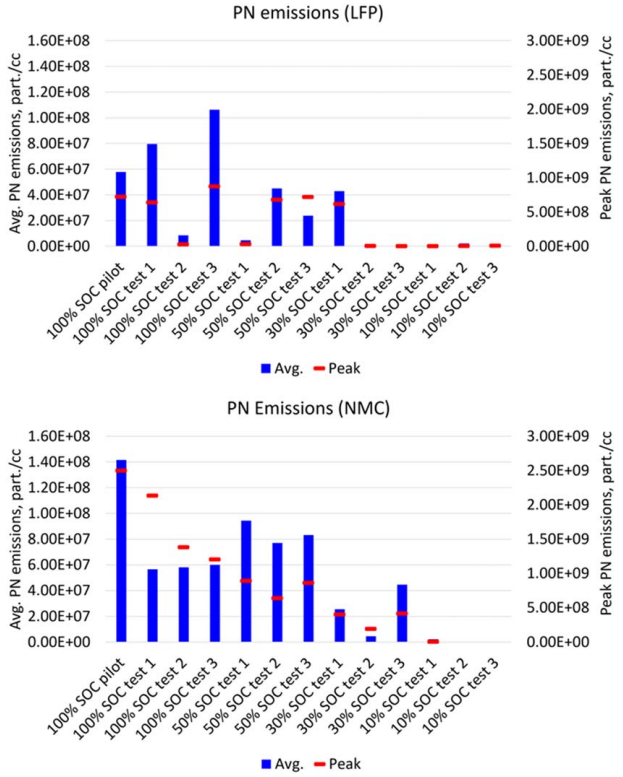

Fig. 9 Average and peak particle number emissions for all tests

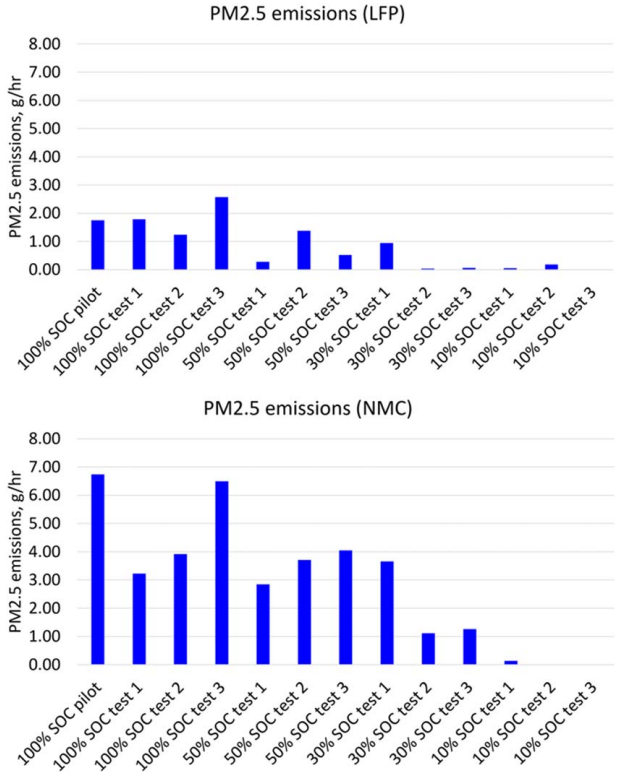

Fig. 10 PM2.5 emissions for all tests

Sierra BG-3 system. Sampling was started during the onset of thermal runaway and stopped either when the pressure drop across the filter reached 34 kPa (the upper threshold beyond which the sample filter will fail) or when PN concentration reported by the DMS500 reached ambient levels.

Figure 10 summarizes the PM2.5 emission rate for all tests conducted. PM2.5 emissions observed during NMC cell failures were higher than those observed with LFP tests. As observed with black carbon and PN emissions, LFP tests conducted at the same SOC exhibited variability in PM2.5 emissions. For both cell chemistries, 100% SOC resulted in higher PM2.5 emissions on an average basis, followed by 50%, 30%, and 10% SOCs. This trend suggests that higher SOC results in a more dramatic failure event with more ejecta release, which has been observed by other researchers. Additional research needs to be conducted to determine the composition and morphology of PM2.5 collected on the filters, which is beyond the scope of this program.

3.5 Size Signatures of Particulate Emissions. Size distributions of thermal runaway emissions were characterized using the DMS500 Fast Particle Analyzer. Figure 11 provides size signatures for both cell chemistries at various SOCs tested. Figure 12 summarizes the geometric mean number diameters of the size signatures for all tests conducted. One significant conclusion that can be drawn is the fact that the particulates emitted from cell failure were well within the human respirable size range. Further, high levels of emissions were also observed in the ultrafine particulate size range. These are defined as sub-100-nm particles and are known to be more toxic to human health as they tend to penetrate deeper into the human respiratory system and eventually diffuse into the bloodstream and reach various organs. In addition to the physical characteristics of these particulates, the chemical composition plays a critical role in terms of their impact on human health. For instance, cobalt is known to be poisonous, and its ingestion could lead to cardiomyopathy and a host of other health conditions that include nerve, vision, hearing, and thyroid problems [24]. Likewise, inhalation of nickel could lead to respiratory and neurological illnesses, in addition to nickel being a known carcinogen [25]. Figure 12 suggests that higher test-to-test variability in GNMD was observed during LFP tests at a given SOC compared to NMC tests. Also, NMC tests resulted in particle size signatures

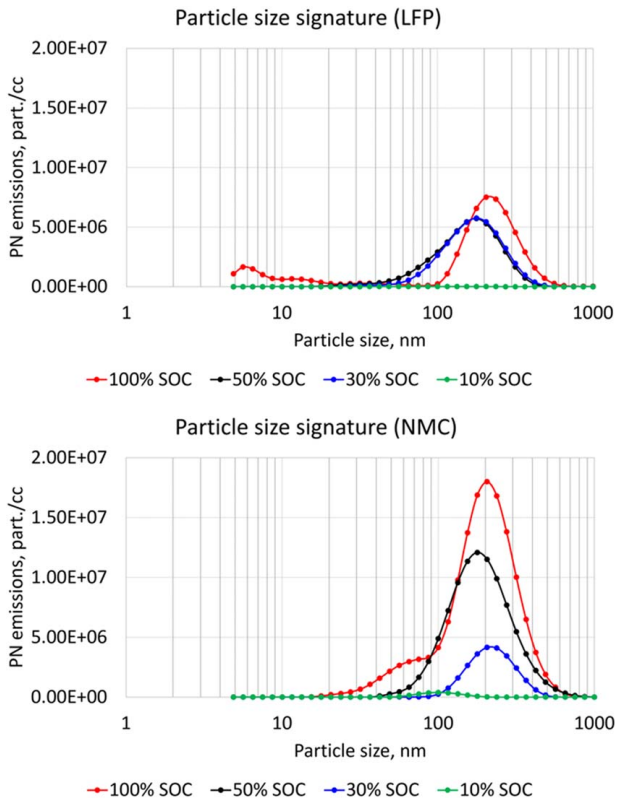

Fig. 11 Size signature of particulate emissions for all tests

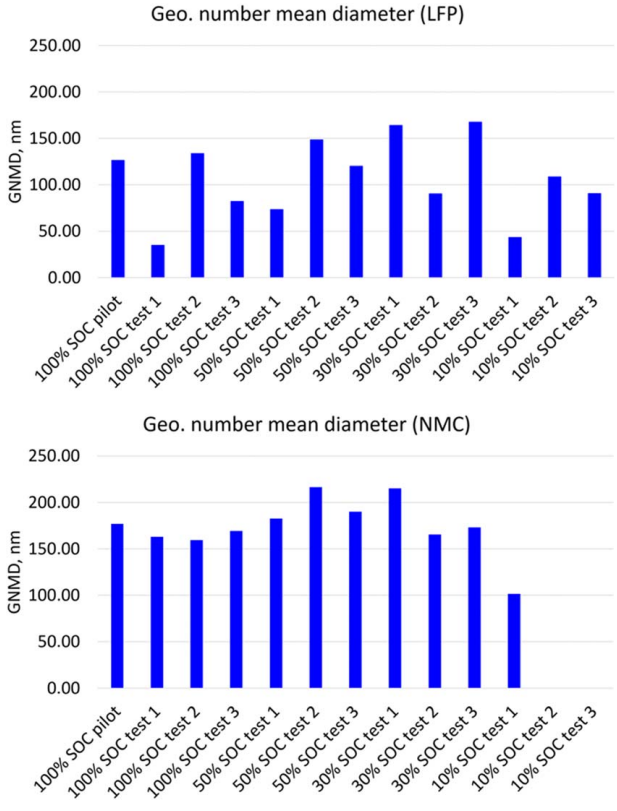

Fig. 12 Geometric number mean diameter analysis of size signatures for all tests

with larger size modes. Interestingly, for both cell chemistries, a decrease in SOC did not dramatically change the size signature, but instead, resulted in changes in peak levels.

4 Conclusions

The focus of this program was to conduct a detailed investigation of particulate emissions from Li-ion cell failure. Two commonly used Li-ion cell chemistries, LFP and NMC, were included as a part of this program. The LFP cells were prismatic metal can cells, while the NMCs were prismatic pouch cells. Cells were induced into thermal runaway using heating as the abuse method for all tests conducted. The test matrix was designed to gain knowledge of the impact of cell chemistry and SOC on thermal runaway particulate emissions and to understand the repeatability/variability associated with cell failure events. For each cell type, three repeats of overheat failure tests were conducted at 100%, 50%, 30%, and 10% SOCs. All tests were conducted in a blast chamber equipped with an exhaust pipe from which particulate emissions were sampled from inception to completion of the thermal runaway process. Real-time black carbon emissions, PN, and size distribution were measured, along with PM2.5, using state-of-the-art instrumentation. Results suggest the following:

- Thermal runaway of the cells tested as part of this program resulted in a significant release of particulate emissions. Peak PN concentrations of the order of $1 \times 10^{+09}$ were 6 orders of magnitude higher than typical ambient PN concentrations. Likewise, peak black carbon levels (~40 mg/m^3 observed during some tests) were also much higher than safe human exposure limits.
- Cell form factor, design, chemistry, composition of electrodes and electrolytes, and capacity could influence emission levels. At 100% SOC, NMC tests yielded average black carbon levels of ~2.2 mg/m^3, PN levels of $\sim 6 \times 10^{+07}$ part/cc, and PM2.5 emissions of ~5.1 g/h. For tests conducted with LFP cells at 100% SOC, average black carbon levels ranging from 0.1 to 0.25 mg/m^3, PN levels of $\sim 8 \times 10^{+07}$ part/cc, and PM2.5 emissions of ~1.6 g/h were observed.
- Results from three identical cell abuse tests at each SOC suggest that there can be significant variability in emissions. This observation is valid for both cell chemistries, with LFP cells exhibiting more variability than NMC cells.
- Among NMC tests, higher SOC tests resulted in higher peak PN concentrations. These concentrations were of the order of $1 \times 10^{+09}$ to $2 \times 10^{+09}$ part/cc. PM2.5 emissions also showed an increase with an increase in SOC. In the case of LFP tests, peak PN concentrations were reasonably similar for 100% and 50% tests (of the order of $7 \times 10^{+08}$ part/cc). However, average PN concentrations and PM2.5 decreased with a decrease in SOC.
- Size signatures of the thermal runaway process indicated emissions well within the respirable size range. Further, a large fraction of these particulates was in the ultrafine size range (<100 nm), which is known to have a more adverse impact on human health.

Knowledge of particulate emissions from battery fires is essential to assess the impact such an event would have on personnel in the vicinity, first responders (and their protective gear), operators, and the environment. Such information is also critical to better understand failure modes such as high-voltage arcing and thermal runaway propagation and to develop mitigation strategies. This program serves to address a critical knowledge gap in understanding some aspects of particulate emissions from cell abuse at various states of charge for cells of two different cathode chemistries and capacities. Future research should examine other cell chemistries, formats, abuse mechanisms, and module and pack-level test articles. Further, additional details about particulate emissions, such as composition and morphology, should be examined.

Acknowledgment

This work was supported by Underwriters Laboratories Research Institutes. The authors acknowledge Dr. Imad Khalek (Institute Engineer) for his review and comments on the manuscript. The authors also acknowledge the following SwRI staff members for their contribution in making this program successful—Mr. Mickey Argo (Assistant Manager), Mr. Daniel Preece (Supervisor), Mr. Angel Herrera (Technician), Mr. Taylor Mraz (Technician), Mr. Isaiah Hernandez (Technician), and Mr. Mario Guillen (Staff Technician).

Funding Data

- UL Research Institutes.

Conflict of Interest

There are no conflicts of interest.

Data Availability Statement

The datasets generated and supporting the findings of this article are obtainable from the corresponding author upon reasonable request.

References

[1] Jeevarajan, J. A., Joshi, T., Parhizi, M., Rauhala, T., and Juarez-Robles, D., 2022, "Battery Hazards for Large Energy Storage Systems," ACS Energy Lett., **7**(8), pp. 2725–2733.
[2] Velumani, D., and Bansal, A., 2022, "Thermal Behavior of Lithium-and Sodium-Ion Batteries: A Review on Heat Generation, Battery Degradation, Thermal Runway—Perspective and Future Directions," Energy Fuels, **36**(23), pp. 14000–14029.

[3] Essl, C., Golubkov, A. W., and Fuchs, A., 2020, "Comparing Different Thermal Runaway Triggers for Two Automotive Lithium-Ion Battery Cell Types," J. Electrochem. Soc., **167**(13), p. 130542.
[4] Wang, Q., Mao, B., Stoliarov, S. I., and Sun, J., 2019, "A Review of Lithium Ion Battery Failure Mechanisms and Fire Prevention Strategies," Prog. Energy Combust. Sci., **73**(Special issue Fire Safety), pp. 95–131.
[5] Golubkov, A. W., Fuchs, D., Wagner, J., Wiltsche, H., Stangl, C., Fauler, G., Voitic, G., Thaler, A., and Hacker, V., 2014, "Thermal-Runaway Experiments on Consumer Li-Ion Batteries With Metal-Oxide and Olivin-Type Cathodes," RSC Adv., **4**(7), pp. 3633–3642.
[6] Larsson, F., Andersson, P., Blomqvist, P., Lorén, A., and Mellander, B. E., 2014, "Characteristics of Lithium-Ion Batteries During Fire Tests," J. Power Sources, **271**, pp. 414–420.
[7] Larsson, F., and Mellander, B. E., 2014, "Abuse by External Heating, Overcharge and Short Circuiting of Commercial Lithium-Ion Battery Cells," J. Electrochem. Soc., **161**(10), pp. A1611–A1617.
[8] Larsson, F., Andersson, P., and Mellander, B. E., 2016, "Lithium-Ion Battery Aspects on Fires in Electrified Vehicles on the Basis of Experimental Abuse Tests," Batteries, **2**(2), p. 9.
[9] Nedjalkov, A., Meyer, J., Köhring, M., Doering, A., Angelmahr, M., Dahle, S., Sander, A., Fischer, A., and Schade, W., 2016, "Toxic Gas Emissions From Damaged Lithium Ion Batteries—Analysis and Safety Enhancement Solution," Batteries, **2**(1), p. 5.
[10] Qiu, M., Liu, J., Cong, B., and Cui, Y., 2023, "Research Progress in Thermal Runaway Vent Gas Characteristics of Li-Ion Battery," Batteries, **9**(8), p. 411.
[11] Sun, J., Li, J., Zhou, T., Yang, K., Wei, S., Tang, N., Dang, N., Li, H., Qiu, X., and Chen, L., 2016, "Toxicity, a Serious Concern of Thermal Runaway From Commercial Li-Ion Battery," Nano Energy, **27**, pp. 313–319.
[12] Quant, M., Willstrand, O., Mallin, T., and Hynynen, J., 2023, "Ecotoxicity Evaluation of Fire-Extinguishing Water From Large-Scale Battery and Battery Electric Vehicle Fire Tests," Environ. Sci. Technol., **57**(12), pp. 4821–4830.
[13] Wang, H., Wang, Q., Jin, C., Xu, C., Zhao, Y., Li, Y., Zhong, C., and Feng, X., 2023, "Detailed Characterization of Particle Emissions Due to Thermal Failure of Batteries With Different Cathodes," J. Hazard. Mater., **458**, p. 131646.
[14] Zhang, L., Yang, S., Liu, L., and Zhao, P., 2022, "Cell-to-Cell Variability in Li-Ion Battery Thermal Runaway: Experimental Testing, Statistical Analysis, and Kinetic Modeling," J. Energy Storage, **56**, p. 106024.
[15] Walker, W. Q., Darst, J. J., Finegan, D. P., Bayles, G. A., Johnson, K. L., Darcy, E. C., and Rickman, S. L., 2019, "Decoupling of Heat Generated From Ejected and Non-Ejected Contents of 18650-Format Lithium-Ion Cells Using Statistical Methods," J. Power Sources, **415**, pp. 207–218.
[16] Zhang, Y., Wang, H., Li, W., and Li, C., 2019, "Quantitative Identification of Emissions From Abused Prismatic Ni-Rich Lithium-Ion Batteries," ETransportation, **2**, p. 100031.
[17] Chen, S., Wang, Z., and Yan, W., 2020, "Identification and Characteristic Analysis of Powder Ejected From a Lithium Ion Battery During Thermal Runaway at Elevated Temperatures," J. Hazard. Mater., **400**, p. 123169.
[18] Barone, T. L., Dubaniewicz, T. H., Friend, S. A., Zlochower, I. A., Bugarski, A. D., and Rayyan, N. S., 2021, "Lithium-Ion Battery Explosion Aerosols: Morphology and Elemental Composition," Aerosol Sci. Technol., **55**(10), pp. 1183–1201.
[19] Yang, Y., Fang, D., Maleki, A., Kohzadi, S., Liu, Y., Chen, Y., Liu, R., Gao, G., and Zhi, J., 2021, "Characterization of Thermal-Runaway Particles From Lithium Nickel Manganese Cobalt Oxide Batteries and Their Biotoxicity Analysis," ACS Appl. Energy Mater., **4**(10), pp. 10713–10720.
[20] Premnath, V., Wang, Y., Wright, N., Khalek, I., and Uribe, S., 2022, "Detailed Characterization of Particle Emissions From Battery Fires," Aerosol Sci. Technol., **56**(4), pp. 337–354.
[21] Reavell, K., Hands, T., and Collings, N., 2002, "A Fast Response Particulate Spectrometer for Combustion Aerosols," SAE Trans., pp. 1338–1344.
[22] Schindler, W., Haisch, C., Beck, H. A., Niessner, R., Jacob, E., and Rothe, D., 2004, "A Photoacoustic Sensor System for Time Resolved Quantification of Diesel Soot Emissions," SAE Trans., pp. 483–490.
[23] Fanick, E. R., and Premnath, V., 2020, "Comparison of Partial and Total Dilution Systems for the Measurement of Polycyclic Aromatic Hydrocarbons and Hydrocarbon Speciation in Diesel Exhaust," SAE Technical Paper 2020-01-2190, p. 8.
[24] Wahlqvist, F., Bryngelsson, I. L., Westberg, H., Vihlborg, P., and Andersson, L., 2020, "Dermal and Inhalable Cobalt Exposure—Uptake of Cobalt for Workers at Swedish Hard Metal Plants," PLoS One, **15**(8), p. e0237100.
[25] Genchi, G., Carocci, A., Lauria, G., Sinicropi, M. S., and Catalano, A., 2020, "Nickel: Human Health and Environmental Toxicology," Int. J. Environ. Res. Public Health, **17**(3), p. 679.